DTU Library

Dynamic performance of a novel offshore power system integrated with a wind farm

Orlandini, Valentina; Pierobon, Leonardo; Schløer, Signe; De Pascale, Andrea; Haglind, Fredrik

Link back to DTU Orbit

Dynamic performance of a novel offshore power system integrated with a wind farm

Valentina Orlandini[a,*], Leonardo Pierobon[b], Signe Schløer[b], Andrea De Pascale[a], Fredrik Haglind[b]

[a]*Department of Industrial Engineering, University of Bologna*
Viale del Risorgimento 2, 40136 Bologna, Italy
[b]*Department of Mechanical Engineering, Technical University of Denmark*
Building 403, 2800 Kongens Lyngby, Denmark

Abstract

Offshore wind technology is rapidly developing and a wind farm can be integrated with off-shore power stations. This paper considers as case study a futuristic platform powered by a wind farm and three combined cycle units consisting of a gas turbine and an organic Rankine cycle (ORC) module. The first aim of this paper is to identify the maximum amount of wind power that can be integrated into the system, without compromising the electric grid balance. The stability of the grid is tested using a dynamic model of the power system based on first principles. Additionally, the dynamics of the system is compared with a simplified plant consisting of three gas turbines and a wind farm, in order to identify benefits of the installation of the ORC system. The maximum allowable wind power is 10 MW for a nominal platform load of 30 MW. The results show that the presence of the ORC system allows decreasing frequency oscillations and fuel consumptions of the platform, with respect to the simplified configuration. On the other hand, the dynamic response of the combined cycle units is slower due to the thermal inertia of the heat transfer equipment.

Keywords: Oil and gas, Organic Rankine cycle, Gas turbine, Offshore wind, Integrated system

Nomenclature

Acronyms

BEM   Blade-Element-Momentum

CC   Combustion Chamber

COND   Condenser

G   electric Generator

GT   Gas Turbine

HPC   High Pressure Compressor

HPT   High Pressure Turbine

LPC   Low Pressure Compressor

LPT   Low Pressure Turbine

NPV   net present value

NREL   National Renewable Energy Laboratory

ORC   Organic Rankine Cycle

OTB   Once-Through Boiler

PT   Power Turbine

R   Reliability

SP   set point

T   organic Rankine cycle Turbine

TIT   Turbine Inlet Temperature

WIND   Wind turbine

Greek symbols

λ failure rate [failures/y]

ρ density[kg/m^3]

Symbols

A   flow passage area

c   speed of sound [m/s^2]

H   pump head [m]

I_t turbulence intensity [-]

I_{TOT} total investment cost [\$]

$\dot{m}$ mass flow rate [kg/s]

M_a Operating and maintenance costs factor that accounts [-]

N   rotation speed of the shaft [rpm]

2

n	number of years
h	specific enthalpy [kJ/kg]
hu	capacity factor [h/yr]
p	pressure [bar]
P_n	maximum wind power installable
q	interest factor
R_i	annual incomes[\$]
s	specific entropy [kJ/kgK]
T	Temperature [C]
V	wind speed velocity [m/s]

Subscripts

CO_2	carbon dioxide
des	design
ng	natural gas
in	inlet section
th	in the throat section
el	electric
GAS	exhaisted gas
out	component discharge
ref	reference

1. Introduction

Offshore oil and gas facilities use inefficient power systems to supply the energy demand on board. The primary objective of platform operators is to ensure a continuous fuel production with minimum risk of failure for the plant. Gas turbines (GTs) are the leading technology on-board offshore platforms since they offer high reliability, compactness and dynamic flexibility. On the other hand, the large ratios of the work-to-heat demand impede to adequately use the exhaust energy for heating purposes. Moreover, conservative operational strategies further deteriorate the energy conversion efficiency during part-load activities.

Pollutant reduction and sustainable production are slowly arising as important concerns in the oil and gas sector [4]. Carbon tax on combustibles has constituted the primary resource for governments to explore the vast potentials in fuel saving and efficiency increase. For instance, Norway levies carbon tax on hydrocarbon fuels since 1991. In 2013, the Norwegian parliament adopted a forceful measure to alleviate the environmental footprint in the oil and gas industry by doubling the taxation to 55 $ per ton of carbon dioxide (CO_2) [32]. A direct remedy is the removal of on-board power generators by relaying on conveyance of electricity from onshore. Recent surveys [2, 17] and operational experience on actual facilities (e.g. the Troll A platform in the North Sea [22]) have proved the economic feasibility of high-voltage direct current systems for low transportation ranges ($\approx 300\,\text{km}$). Capturing and storing the CO_2 is also a solution to reduce emissions offshore. Floating plants with large power outputs (up to 450 MW) for offshore electrification integrating compression, pre-conditioning and CO_2 capture are under investigation [19, 45]. A drawback is that the sequestration process penalizes the energy conversion efficiency (up to 9 %-points [19]). Furthermore, this process does not cope with the removal of other pollutants such as sulfur and nitrogen oxide.

A solution to enhance the system performance is the implementation of a waste heat recovery unit at the bottom of the gas turbines. A mature technology is the steam Rankine cycle (SRC). Kloster [24] described the existing SRC units in the Oseberg, Eldfisk and Snorre B offshore installations. Air bottoming cycles (ABCs) are an alternative to SRC units as they employ a non-toxic and inflammable working fluid. Moreover, ABC power modules do not require a condenser as they operate as open-cycles. This feature leads to high compactness and low weight. Various studies focused on the implementation of ABC units offshore. The results proved a low gain in performance despite the low weight and short pay-back time [7, 36, 5]. Organic Rankine cycle power systems have recently emerged as suitable technology [39, 6]. Favorable design features are the high modularity, compactness and low weight. With ORCs, improvements of the energy conversion efficiency range from 10 % to 20 %, with an additional specific weight of 15 - 20 $\text{t} \cdot \text{MW}^{-1}$ [38].

Research efforts focuses on integrating wind power in oil and gas facilities. The rapid development of offshore wind power technologies enables designing floating turbines for water depths up to 700 m [43] and distances from the coast of around 100 km (case of BARD Offshore 1 [27]). The solution is attractive due to the uniform distribution of wind speed and space

4

availability. The integration does not require additional weight and space compared to the implementation of waste heat recovery units or carbon capture technologies. On the other hand, additional challenges related to the stability of the electric network arise, due to the variability of this renewable source. As an example, Årdal et al. [1] and Marvik et al. [31] studied how the presence of wind turbines could improve the stability of an offshore oil and gas platform using voltage controllers. Similarly, He et al. [18] investigated the integration between an offshore oil and gas platform and an offshore wind farm. To the authors' best knowledge, in all previous studies addressing the integration of wind farms on offshore platforms, the platform power plants consist of gas turbines only.

The objective of this paper is to study the dynamic performances of a pioneering oil and gas platform. The stand alone power station comprises an offshore wind farm and three gas turbines, each one coupled with an ORC module. In particular, we aim at answering two research questions: i) what is the maximum number of wind turbines for which the stability of the platform electric grid is not compromised?, and ii) is the implementation of the ORC units beneficial for the plant flexibility? A dynamic model of the power system based on first principles is developed using the Modelica language. The model is integrated with a time series-based model of offshore wind mills. Dynamic tests, e.g., the loss of wind power, are performed to determine the maximum frequency excursions and the variations of control and process variables. These simulations allow identifying a reasonable size of the wind farm. Additional tests are performed using only the gas turbines to evaluate the effect of the ORC units on the system dynamics.

This paper is structured as follows: Section 2 deals with the description of case study, while Section 3 presents the models of the system components. Section 4 reports the results and discussions. Conclusive remarks are given in Section 5.

2. Case study

This paper considers a generic the upgrading of an existing offshore oil and gas platform located in the North Sea. The floating wind turbines are connected to the stand alone electric grid, see Figure 1(a). The wind turbine considered in this work is a reference generator developed at the National Renewable Energy Laboratory (NREL) [23]. The wind turbine is a three-blade upwind variable-speed and variable blade-pitch-to-feather-controlled turbine. The

NREL together with the Massachusetts Institute of Technology is studying a tension leg platform for a floating wind turbine. Pretensioned mooring lines anchored to the seabed by suction piles [8] will connect the corners of the platform, designed for water depths from 60 m to 200 m and for a 5 MW turbine. The on board power plant consists of three combined cycle systems, as shown in Figure 1(a). Each one comprises a GT topping module and an ORC bottoming cycle unit. Figure 1(b) shows the layout of the combined cycle unit. The ORC turbogenerator recovers the heat from the exhaust gases of a gas turbine. The SGT-500 gas turbine is considered as topping unit. This engine has been widely adopted and commonly installed on offshore platforms requiring high fuel flexibility and reliability. The turbine blades are uncooled. The engine employs two coaxial shafts coupling the low pressure compressor (LPC) with the low pressure turbine (LPT) and the high pressure compressor (HPC) with the high pressure turbine (HPT). The power turbine (PT) transfers mechanical power through a dedicated shaft to the electric generator (G1). Natural gas is the fuel used in the combustion chamber (CC). Table 1 reports the design-point specifications of the gas turbines as provided by the manufacturer for the C-version lunched in the 80's.

The ORC unit comprehends the single-pressure non-reheat once-through boiler (OTB), the turbine (T), the sea-water cooled shell-and-tube condenser (COND) and the feed-water pump (P). The working fluid is benzene (molecular weight $78.11\,\mathrm{g \cdot mol^{-1}}$, critical temperature and pressure $288.9\,°\mathrm{C}$ and $49.9\,\mathrm{bar}$). This compound is widely adopted for operating ORC systems in this range of temperature, see, e.g., Colonna et al. [13]. The high resonance stabilization energy of the aromatic structure ensures its chemical stability up to $315\,°\mathrm{C}$ [3]. The saturation curve of benzene is positive (dry fluid). A shell-and-tube recuperator is added to decrease the energy contained in the superheated vapor exiting the ORC expander. The in-house simulation tool developed by Pierobon et al [39] is used to design the ORC unit. The software allows identifying the thermodynamic states at the inlet and outlet of each component applying basic energy and mass balances, once defined the boundary conditions. Subsequently, the design of the plant equipment is carried out automatically, ultimately leading to the evaluation of the chosen performance metrics. An iterative procedure, based on the genetic algorithm method explores the design space, looking for optimal design configurations. Table 2 reports the main parameters assumed for the considered ORC system, according to the described methodology.

6

3. Methods

This part of the paper gives an overview of the adopted modeling language, see Section 3.1. Sections 3.2 and 3.3 present the models of the gas turbine and organic Rankine cycle unit. Section 3.4 describes the model of the wind farm used to calculate the power provided by the floating turbines.

3.1. The modeling language

The dynamic model of the power system is developed using components from existing Modelica packages [11]. Modelica is an object-oriented modeling language that allows building dynamic models using an equation-based modular approach.

The gas turbine sub-system model is built by exploiting basic components included in the ThermoPower library [11]. The model of the ORC system adopts software objects from the Modelica ORC package [12], with suitable adaptations regarding the heat transfer coefficients and flow configuration in the once-through boiler.

3.2. The gas turbine

Figure 2 shows the Modelica object diagram of the gas turbine. Compressors and turbines are multi-stage machines modeled as zero-dimensional components using steady-state off-design characteristics. The low and high pressure compressors are modeled based on maps of axial compressors provided by Kurzke [25]. These maps, originally from Carchedi and Wood [10], use tables that state values for flow coefficient, pressure ratio, isentropic efficiency and speed of revolution for the complete operating range. The maps are scaled following the methodology proposed by Kurzke [26]. The equation proposed by Stodola [44] is employed for modeling the low pressure, high pressure and power turbines. This equation expresses the relation between the inlet and outlet pressure of the expander with the mass flow rate and the turbine inlet temperature in off-design conditions. The turbine off-design efficiency is predicted with the correlation proposed by Schobeiri [42].

The combustion chamber (CC) unit is built assuming complete and adiabatic combustion process. In the component, mass and energy conservation are expressed including the dynamic terms. As suggested by Camporeale et al. [9], the mass and the internal energy are computed using the thermodynamic properties of the combustion products exiting the burner. Furthermore, it is assumed that the combustion process and the mixing action take place at constant

7

volume. This parameter is set according to the data provided by the gas turbine manufacturer. The pressure drops are lumped in an external device. In off-design conditions, a quadratic dependence to the volumetric flow rate is assumed.

The shaft dynamic balance is used to model the dynamics of each spool. The values of the inertia of the rotating masses (shaft, blades, generator) are set according to data provided by the gas turbine manufacturer. The part-load performance of the electric generator is predicted using the equation proposed by Haglind and Elmegaard [16], where the electric efficiency in off-design is evaluated as function of load and copper loss fraction. Figure 2 shows (on the topside) the control system of the SGT-500 engine as given by the manufacturer. The compressors are not equipped with variable inlet guide vanes. The load of the engine can be adjusted by varying the opening of the fuel valve. The reader can refer to Pierobon et al. [37] for an in-depth description of the control system blocks. The cited reference presents also the validation of the dynamic model of the SGT-500 engine based on data provided by the gas turbine manufacturer. The off-design steady-state behavior of the gas turbine model is compared to the part-load characteristics given by the manufacturer in 10% and 100% range. The mass flow rate and temperature of the exhaust gases, fuel mass flow rate and pressure in the combustion chamber are considered. The quantity showing the larger mismatch is the mass flow rate of the combustible. The relative error is about 3% for loads larger than 60% and it increases up to 15% when the load decreases to 10%. Based on these results, the developed gas turbine model is able to reproduce both the steady-state and the dynamic behavior of the components with reasonable accuracy, over the entire range of loads encountered during real operation [37].

3.3. The organic Rankine cycle system

The once-through boiler, shown in the object diagram of Figure 3, is implemented by combining basic ThermoPower modules. Figure 4 shows the 1D flow models for the gas side (top) and fluid side (bottom of the figure), and the 1D thermal model for the tube bundle (middle). The exchange of thermal power is modeled with so-called 1D thermal ports (in orange in the figure). The counter-current model establishes the topological correspondence between the control volumes on the tube walls, and the control volumes on the gas flow model. The tube metal wall of the boiler is modeled by a 1D dynamic heat balance equation, discretized by finite volumes. The flow models contain one-dimensional dynamic mass and energy balance equations, discretized by the finite volume method, assuming a uniform pressure distribution.

8

The relatively small friction losses are lumped in an external component. The pressure drops in off-design conditions are estimated assuming a quadratic dependency with the volumetric flow rate. The thermal resistance in the radial direction and thermal diffusion in the axial direction are neglected due to the relatively small contribution, as described by Casella et al. [12]. The heat transfer coefficient between the gas and the outer pipe surface is much lower than the one between the inner pipe surface and the ORC working fluid. Therefore, the overall heat transfer is essentially dependent on the flue gas side only.

The heat transfer coefficient at the interface between the flue gas and the metal wall, in off-design conditions, is evaluated with the relation proposed by Incropera et al. [20]

$$h = h_{\text{des}} \left(\frac{\dot{m}}{\dot{m}_{\text{des}}} \right)^n \ , \tag{1}$$

where h is the heat transfer coefficient, $\dot{m}$ the mass flow rate, and the subscript "des" refers to the value at nominal operating conditions. The variable n, taken equal to 0.6, is the exponent of the Reynolds number in the heat transfer correlation. The thermal interaction between the wall and the working fluid is described by specifying a sufficiently high constant heat transfer coefficient.

The turbine is modeled as an equivalent chocked de Laval nozzle. The throat flow passage area is the sum of the throat areas of the nozzles that constitute the first stator row. An isentropic expansion is assumed from the inlet section to the throat, where sonic conditions are attained. The corresponding system of equations is listed below.

$$\begin{cases} s_{\text{in}} = s(p_{\text{T,in}}, T_{\text{T,in}}) \\ h_{\text{S,th}} = h_{\text{T,in}}(p_{\text{T,in}}, T_{\text{T,in}}) - \frac{1}{2} \cdot c\,(h_{\text{S,th}}, s_{\text{in}})^2 \\ \dot{m} = \rho_{\text{S,th}}(h_{\text{S,th}}, s_{\text{in}}) \cdot c\,(h_{\text{S,th}}, s_{\text{in}}) \cdot A_{\text{th}} \ , \end{cases} \tag{2}$$

where s_{in} is the specific entropy at the turbine inlet. The subscripts "S,th" and "T,in" indicate static conditions in the throat section and total conditions in the expander inlet section (i.e. total inlet pressure $p_{\text{T,in}}$ and total temperature $T_{\text{T,in}}$), respectively. The specific enthalpy and the speed of sound are named h and c. The variables $\dot{m}$, ρ and A_{th} are the mass flow rate through the nozzle, the density and the flow passage area. The throat passage area is a fixed parameter obtained from the design calculation. Equation 2 relates to the mass flow rate and the turbine inlet conditions at part-load. The off-design isentropic efficiency is predicted with the correlation proposed by Schobeiri [42].

9

The recuperator is modeled by the counter-current connection of 1D ThermoPower modules, much as the once-through boiler, see Figure 4. The heat transfer on the vapor side dominates. Therefore, the overall heat transfer coefficient is taken equal to that at the interface between the organic vapor and the metal wall. The overall heat transfer in off-design conditions and the pressure drops are modeled as for the once-through boiler.

The condenser is trivially modeled as a fixed pressure component. This assumption is justified considering the large availability of sea-water. The cooling circuit can thus be controlled in such a way that the condenser pressure is nearly constant. For simplicity, the condensate is assumed to leave the component in saturated conditions (no subcooling) with no pressure losses.

The pump model is based on a head-volume flow curve derived by fitting the data of an existing centrifugal pump designed for similar volumetric flows and heads. The curve, given as a function of $\phi = \dot{m}/\rho \cdot \rho_{\text{des}}/\dot{m}_{\text{des}}$ and the rotation speed of the shaft N, is expressed as

$$H = H_{\text{des}} \cdot \left(b_1 + b_2 e^\phi\right) \cdot \left(\frac{N}{N_{\text{des}}}\right)^2, \tag{3}$$

where H is the head, $b_1 = 2.462$, and $b_2 = -0.538$. The exponential functional form is selected in order to result in a monotonic relation. This formulation increases the model robustness compared to polynomial expressions. The isentropic efficiency of the pump is expressed as a function of the coefficient $F = \phi \cdot N_{\text{des}}/N$, using the methodology proposed by Veres [46]. The off-design electric efficiency of the ORC generator is calculated similarly to the gas turbine generator. The electro-mechanic efficiency of the pump motor is evaluated by assuming a quadratic dependency on the ratio between the actual load and its nominal value. Figure 3 shows also the ORC control system, consisting of a proportional-integral (PI) controller. This component adjusts the speed of the pump to maintain the temperature at the inlet of the expander (TIT in Figure 3) equal to the design-point value (SP_TIT in Figure 3). This strategy, currently used in ORC turbogenerators [12], ensures safe activities by tracking the hottest fluid temperature of the thermodynamic cycle.

The model of the ORC system is made of software objects acquired from a library that was developed to model a $150\,\text{kW}$ ORC turbogenerator using toluene as the working fluid. This was successfully validated for dynamic operation against experimental data [12]. The model of the bottoming cycle unit is, therefore, deemed reliable, considering the similarity of the application at hand with the one presented in the cited reference.

3.4. The wind farm

Figure 5 reports the wind speed probability curve. The data are representative for the North Sea. A wind speed of $9\,\text{m} \cdot \text{s}^{-1}$ is chosen as average wind speed, since it has the highest probability of occurrence, equal to 0.35, as shown in Figure 5. The turbulent wind is created by the IEC Turbulence Simulator in the WAsP Engineering model using the Mann model [29]. The turbulence intensity, I_t, is calculated using the normal turbulence model [21], as following

$$I_t = \frac{I_{\text{ref}}(0.75 \cdot V + 5.6[m/s])}{V} \,, \tag{4}$$

where V is the wind speed velocity in m·s^{-1} and $I_{\text{ref}} = 0.14$ is the expected value of the turbulence intensity at a wind speed of $15\,\text{m} \cdot \text{s}^{-1}$ for medium turbulence characteristics [21]. Hence, at $9\,\text{m} \cdot \text{s}^{-1}$, I_t results equal to 0.19.

Considering a NREL 5 MW wind turbine, the output power is calculated by the aeroelastic code Flex5 [35]. This code is widely used in the industry to model the dynamics of the wind turbine and monopile foundation. The aerodynamic loads on the blades are calculated by the unsteady blade-element-momentum (BEM) method.

The wind instantaneous speed and the power production of the wind generator are obtained for one hour, considering a time step equal to 0.02 sand processed as described in Section 4.2.

3.5. Economic evaluation

The economic evaluations are based on the net present value (NPV) method. The NPV is calculated considering the equipment lifespan n, the interest factor q, the total investment cost I_{TOT} and the annual income R_i. Moreover, M_a is a non-dimensional factor that accounts for operating and maintenance costs.

$$NPV = \sum_{i=1}^{n} M_a \frac{R_i}{(1+q)^i} - I_{TOT} \,. \tag{5}$$

The major sources of annual incomes are associated with the fuel savings and with the avoided CO_2 taxes, respectively named R_{ng} and R_{CO2}, evaluated as

$$R_{ng} = c_{ng} v_{st} \Delta \dot{m}_{ng} h_u \,, \tag{6}$$

$$R_{CO2} = c_{CO2} \Delta \dot{m}_{CO2} h_u \,, \tag{7}$$

11

where c_{ng} is the price of natural gas, v_{st} is the fuel specific volume calculated at 15 °C and 1.013 bar, $\Delta \dot{m}_{ng}$ is the fuel saving and h_u represents the capacity factor in h/yr. In eq. (7), c_{CO2} represents the carbon dioxide tax and $\Delta \dot{m}_{CO2}$ is the avoided CO_2 emission.

3.6. Reliability analysis

In the reliability analysis the reliability of a single component $R(t)$ is defined as the probability that it does not fail in a considered time range t, assuming that it is working at the beginning of that time interval [15]. Generally, $R(t)$ can be calculated using the failure rate λ, as shown in eq. (8) [41]. A parallel system configuration can work as long as not all components of the system fail. Conceptually, in a parallel configuration the total system reliability is higher that the reliability of any single system component. The reliability of a system placed in a parallel configuration $R(t)_{parallel}$ can be evaluated follow eq. (9) [15], where n is the number of installed components. Meanwhile, a series system is a configuration such that, if any one of the system components fail, the entire system fails. Conceptually, a series system is one that is as weak as its weakest link [41]. The reliability of a series system $R(t)_{series}$ is evaluated based on eq. (10), where m is the number of components set in series. Moreover, the failure rate of the entire system is equal to the sum of the components failure rates. Meanwhile eq. (11) evaluates the reliability of a redundant-parallel system consist of l components, supposing a perfect switch between the different conditions [15].

$$R(t) = e^{-\lambda t} \tag{8}$$

$$R(t)_{parallel} = 1 - \prod_{i=1}^{n} (1 - R_i(t)) \tag{9}$$

$$R(t)_{series} = \prod_{i=1}^{m} R_i(t) \tag{10}$$

$$R(t)_{redundant-parallel} = e^{-\lambda t} \cdot (1 + 2\lambda t + \frac{(\lambda t)^2}{2!} + \cdots + \frac{(\lambda t)^l - 1}{(l-1)!}) \tag{11}$$

While a full reliability analysis is out of the scope of this paper, a few simplified considerations wil be done in section 4.1.1 regarding the system reliability, following the existing literature which provides statistical information on the components failure rates.

4. Results and discussion

Section 4.1 presents the simulation results used to identify the maximum wind power installable on-board. The selection criteria are the standards specified for offshore stand-alone electric grids. Sections 4.2 and 4.3 analyze the plant flexibility and the energy savings during the wind power fluctuations.

4.1. The maximum allowable wind power

The electric power required by the oil and gas platform is assumed constant and equal to 30 MW. This nominal demand is a reasonable figure for offshore facilities in the North Sea [33]. The power system on board (three combined cycle units) has a total installed capacity of 64 MW. Two combined cycle units run at a time covering 50 % of the load each. The third unit is on stand-by. Having an excess power capacity allows the platform operator to: i) minimize the risk of failure of the plant and causing a halt of oil production, and ii) cope with possible variations in the power demand during the reservoir lifetime. This plant arrangement is commonly adopted in offshore power stations in order to enhance the system reliability and ensure the necessary reserve power for peak loads. The sudden loss of wind power is the worst possible scenario the plant has to withstand without compromising the functionality of the power system. The scenario implies that the wind turbines provide their maximum power output and the two combined cycle plants supply the remaining power until 200 s, when, in 1 s, the wind power production drops to zero. As a consequence, the GT+ORCs have to increase the load to match the total power demand and stabilize the grid frequency. The maximum absolute frequency change has to be lower than 5 %, as imposed by the NORSOK standard [34]. This dynamic metric is thus used to identify the maximum wind power $\dot{P}_n$ installable on board.

The possible scenarios are:

- case 1: one wind turbine installed ($\dot{P}_n$= 5 MW),

- case 2: two wind turbines installed ($\dot{P}_n$= 10 MW),

- case 3: three wind turbines installed ($\dot{P}_n$= 15 MW).

Figure 6 shows the frequency dynamics for the three test cases. The plot reports also the maximum allowable undershooting (red dotted line). All curves exhibit an undershooting, caused

13

by the increased load demand. Figure 6 demonstrates that case 3 is not feasible as the frequency exceeds the prescribed threshold. Therefore, the integration of three wind turbines is not acceptable for the stability of the grid. The second dynamic metric used to compare the three cases is the rise time. This quantity is defined as the time required for the frequency to return back to 99 % of the value at steady-state (50 Hz). Case 1 and 2 present faster responses than case 3, with a rise time of 2 s and 8 s, respectively. Case 3 presents a rise time of 11 s, as visible in Figure 6. Two wind turbines are installable since they can supply one third of the electric load on the platform (30 MW) without compromising the stability of the electric grid.The optimal ratio strongly depends on the: i) maximum frequency tolerance, ii) control system of the gas turbine, and iii) size of the wind turbine. The results obtained in this paper are generally applicable to the North Sea region given the selected grid specifications and the adopted offshore wind turbines.

Figure 7 shows the trend of the temperature at the inlet of the ORC expander during the loss of the wind powerin the three analyzed cases.This variable is of paramount importance, being closely related to the maximum temperature reached by the ORC working fluid. Its thermal stability is a major concern in the design of ORC systems. The fluid decomposition can compromise the integrity and the performance of the components. The plot demonstrates that the peak value of the temperature in case 2 is equal to 314.9 °C. This is acceptable for the thermal stability of benzene. Andersen et al. [3] demonstrated that the decomposition is negligible for operating temperatures lower than 315 °C.

4.1.1. Plant reliability

The sizing of the wind farm following the methodology described in section 4.1 allows to get an integrated system able to satisfy at each time the required load. Moreover, the power plant operation results independent from the wind turbines failures. From the definition of reliability $R(t)$ given in section 3.6, the platform power plant and the wind farm could be viewed as two different systems in a reliability analysis. Indeed, as previously described, in the case of the sudden loss of wind power the platform power plant is able to withstand without compromising the functionality. An estimation of wind turbines and combined cycles reliability can be performed. The yearly failure rate λ_{WT} of each wind turbine can be set equal to 2.38 (failures per year) according to Prez et al. [40], mainly related to faults in the electrical, control, sensors and hydraulic systems. This quite high value among data for wind turbines available

in literature can be considered because larger wind turbines tend to fail more frequently than smaller ones [40]. The reliability of the overall wind farm in the analyzed case can be evaluated considering the wind turbines placed in a parallel configuration, because the wind farm results out of service when both the mills are broken. Thus, as described in section 3.6, the wind farm yearly reliability results equal to 0.177. The platform power plant operational configuration, shown in fig. 1, can be schematically considered as three series of two combined cycle (i.e. the series are combined cycle 1 and 2, combined cycle 2 and 3, combined cycle 1 and 3) set in parallel. The failure rate of each combined cycle λ_{CC} is set equal the gas turbine failure rate. The gas turbine critical failure rate per 10^6 hours is reported in literature between 460 and 1700 according to statistical data on real machines [30]. Therefore, considering a low yearly GT failure rate equal to 4.03, the reliability of two gas turbines set in series results equal to $3.16 \cdot 10^{-4}$. For the entire platform power plant the reliability is equal to 0.013 and considering a perfect switching between configuration, due to the presence of the third GT+ORC combined cycle unit maintained in stand-by. Finally, the wind farm and the combined cycle reliability values could be evaluated considering more variables, as the electrical infrastructure generally split in three sub sections, e.g. export cables, inter-array cables and the offshore substation. The offshore substations are used to reduce electrical line losses and improve the overall electrical efficiency by increasing the voltage level from the collection system and then exporting the power. Moreover, they contains the necessary switching panels and other electrical facilities (e.g., power factor correction systems) [28].

4.2. Plant flexibility

This section aims at evaluating the capability of the power system to rapidly adapt to an electric grid with varying production of wind power. Given the results presented in Section 4.1, two wind turbines are connected to the grid. Figure 8 shows the production data of the two generators, named WT1 and WT2. The time range is equal to 200 s. This time is long enough to evaluate the dynamics of the integrated system. The values given in the plot are derived from the data computed as described in Section 3.4. The data collected for the first 30 minutes are used to reproduce the WT1 wind fluctuations. The data collected for the remaining time are used for the WT2. The production data are integrated in the plant model using a time-step of 1 s. The dynamics of the power system is also assessed for the three gas turbines without waste heat recovery unit. This allows quantifying the impact of the ORC units on the dynamic

15

flexibility of the system. The two plant configurations under investigation are:

- configuration A: the wind farm is coupled to three combined cycle units,

- configuration B: the wind farm is integrated with three gas turbines.

In both cases, two units run at the same time covering 50 % of the required power each. The third engine is on stand-by. The power demand on board is constant and equal to 30 MW in the two configurations. Figure 9(a) shows the power produced by the five electric generators connected to the grid (configuration A). The gas turbines and the ORC modules produce 62 % and 18 % of the total demand. The wind mill supplies the remaining 20 %. Figure 9(b) shows that the gas turbines have to cover around 80 % of the total required power as for configuration B.

Figure 10 shows the frequency trends of the two configurations as a function of time. The presence of the organic Rankine cycle units reduces the small frequency oscillations compared to the use of two gas turbines alone. On the other hand, the maximum frequency variations are higher in case of ORCs installation. Figure 11 reports the mechanical power produced by the topping and bottoming units, i.e., $\dot{P}_{\mathrm{m,GT}\_}A$ and $\dot{P}_{\mathrm{m,ORC}}$, considering configuration A, and the mechanical power produced by the gas turbine, i.e., $\dot{P}_{\mathrm{m,GT}\_}B$, considering configuration B. The reported data refer to one combined cycle unit in configuration A and to one gas turbine in configuration B.

The plot pinpoints that the fluctuations of wind power do not influence the power produced by the ORC turbine. The maximum $\dot{P}_{\mathrm{m,ORC}}$ variation is lower than 0.2 MW. This trend is due to the inertia of the heat transfer equipment included in the ORC turbogenerator. The GTs are thus responsible for satisfying the load demand and cope with the wind power variability.

Figure 12 shows the variation of the mechanical power produced by the gas turbines with respect to the steady-state value for configuration A and B. In Figure 12, the area under the red and black curves is equal to 176 MJ and 191 MJ. These values are related with the kinetic energy stored into the rotating masses. The use of the ORC units enables reducing the variation of the mechanical power produced by the gas turbines, but it reduces the kinetic energy stored in the system. This smooths the dynamics of the fuel valve and reduces the smallest oscillations of the frequency. Note that the manufacturer designed the control system for the operations of the sole gas turbines. The implementation of the ORC turbogenerators may require a further

16

tuning of the controller, thus improving the system dynamics. Moreover, the reliability of the system in configuration A could be a problem with respect to the system in configuartion B, due its more complexity. These aspects are, however, beyond the scope of the present work. All the presented results suggest that the ORC systems enable decreasing the amplitude of the valve regulation. For the given load change, the response of gas turbines in configuration B is quicker than in configuration A. Therefore, the integrated system in configuration A is less capable to follow the wind fluctuations compared to the plant in configuration B.

4.3. Fuel savings and emission reduction

Figure 13 shows the fuel consumption and the actual CO_2 emissions of the two power systems (configuration A and B). The CO_2 emissions are calculated according to [11], assuming perfect combustion and no heat losses to the environment. Thedifference between two configurations demonstrates that the implementation of the waste heat recovery systems can reduce the fuel consumption and CO_2 emissions by more than 15 %. Namely, the use of ORC units (configuration A) enables the saving of more than 60 kg of fuel and more than 160 kgof CO_2 in a time period of 200 s.

An economic assessment is possible based on the fuel and CO_2 savings. The NPV method (described in section 3.5) is used to assess the economic feasibility of the waste heat recovery units and wind mill. Based on information provided by the platform operator, reasonable figures for the discount rate and the life-time of the investment are 6 % and 30 years. The operating and maintenance costs are also accounted with an appropriate coefficient (M_a in section 3.5 set equal 0.9). The two sources of annual incomes are associated with the fuel savings and with the avoided CO_2 taxes respect to the use of gas turbines only. A fuel price of $0.09\,\$ \cdot Sm^{-3}$ and a carbon dioxide tax of $55.9\,\$ \cdot t^{-1}$ [32] is assumed. The yearly demand of electricity is calculated assuming a constant duty of 30 MW and a capacity factor of 7000 hours per year. The investment cost of the wind turbines per unit of power is equal to 5 \$/W [14], while a specific price of 3 \$/W is considered for the ORC units. The evaluated NPVs are equal to 5.85 M\$ and 3.05 M\$ for configuration A and B.

Figures 14 and 15 show the net present value for configuration A and B as a function of the fuel price and CO_2 tax. The horizontal axis reports the fuel price as a percentage of base case fuel price (100 % correspond to $0.09\,\$ \cdot Sm^{-3}$). In particular, fig. 15 shows the effect of CO_2 tax increase in comparison with the reference CO_2 tax value scenario, while fig. 14 presents the ef-

fect of the CO_2 tax decreasing. In fig. 15 the solid lines refer to the tax scenario in the base case (named respectively base case-configuration A and base case-configuration B). The dotted and dashed lines refer respectively to a no-tax scenario and to a 50 % tax scenario for the considered configurations. Similarly, the solid lines in fig. 14 refer to the base case tax scenario, while the dotted and dashed lines present respectively the results of an increase of the 50 % and of the 100 % of the CO_2 tax. The plots show how configuration A becomes more convenient with respect to configuration B when the fuel cost increases. However, in a no-tax scenario or in the case of a low fuel price, configuration B is more attractive, due to the high investment cost of the ORC units. As reported in Figure 15, increasing the carbon tax price give an opposite trend: the NPV achievable using configuration A are higher than using configuration B also for cheap fuel scenarios.

5. Conclusions

This paper presents a dynamic study of a novel offshore power system for oil and gas platforms. More in detail, the power system on board consists of three gas turbines each one equipped with an organic Rankine cycle turbogenerator. Wind mills are also connected to the stand-alone electric grid to reduce the fuel consumption and pollutants. The platform considered as case study has a nominal electric power demand of 30 MW, and it is located in the North Sea. A dynamic model of the power system is developed in the Modelica language using component models from validated libraries. The first aim of the paper is the evaluation of maximum allowable wind power for which the stability of the platform electric grid is not compromised. The considered wind turbines have a design capacity of 5 MW and they are sized and modelled on NREL offshore reference generators. While, the second aim of the study is to assess the impact of the ORC turbogenerators on the dynamic flexibility of the power plant.The simulations suggest that the wind millsshould cover not more than one third of the power consumption in nominal conditions. The model allows also estimating the fuel consumption and the CO_2 emissions. The net present value method demonstrates the economic feasibility of the waste heat recovery units and wind mill. The results suggest that the use of the ORC units enables reducing the frequency fluctuations caused by the variability of the wind production, compared to the installation of the gas turbines alone. Conversely, the waste heat recovery system makes the plant slower due to inertia of the heat transfer equipment. It is advisable to obtain new

18

control systems to tackle this issue and to cope with the extreme need for reliability. Future work will thus focus on the improvement of the gas turbine control system using model-based regulators, e.g., the model predictive control. Moreover, the use of an electric storage system could be a feasible solution to reduce the grid instability and to improve the efficiency of the overall integrated system.

References

[1] Årdal, A. R., Undeland, T., & Sharifabadi, K. (2012). Voltage and frequency control in offshore wind turbines connected to isolated oil platform power systems. *Energy Procedia*, *24*, 229–236.

[2] de Alegría, I. M., Martín, J. L., Kortabarria, I., Andreu, J., & Ereño, P. I. (2009). Transmission alternatives for offshore electrical power. *Renewable and Sustainable Energy Reviews*, *13*, 1027–1038.

[3] Andersen, W. C., & Bruno, T. J. (2005). Rapid screening of fluids for chemical stability in organic Rankine cycle applications. *Industrial & Engineering Chemistry Research*, *44*, 5560–5566.

[4] Barker, A., & Jones, C. (2013). A critique of the performance of EIA within the offshore oil and gas sector. *Environmental Impact Assessment Review*, *43*, 31–39.

[5] Benato, A., Pierobon, L., Haglind, F., & Stoppato, A. (2014). Dynamic performance of a combined gas turbine and air bottoming cycle plant for off-shore applications. In *Proceedings of the 12th Biennial Conference on Engineering Systems Design and Analysis*. Copenhagen, Denmark.

[6] Bhargava, R., Bianchi, M., Branchini, L., De Pascale, A., Melino, F., Peretto, A., & Valentini, E. (2014). Thermo-economic evaluation of ORC system in off-shore applications. In *Proceedings of ASME Turbo Expo 2014*. Düsseldorf, Germany.

[7] Bolland, O., Førde, M., & Hånde, B. (1996). Air bottoming cycle: use of gas turbine waste heat for power generation. *Journal of Engineering for Gas Turbines and Power*, *118*, 359–368.

[8] Breton, S.-P., & Moe, G. (2009). Status, plans and technologies for offshore wind turbines in Europe and North America. *Renewable Energy*, *34*, 646–654.

[9] Camporeale, S., Fortunato, B., & Dumas, A. (2000). Dynamic modelling of recuperative gas turbines. *Proceedings of the Institution of Mechanical Engineers, Part A: Journal of Power and Energy*, *214*, 213–225.

[10] Carchedi, F., & Wood, G. R. (1982). Design and development of a 12:1 pressure ratio compressor for the Ruston 6-MW gas turbine. *Journal for Engineering for Power*, *104*, 823–831.

[11] Casella, F., & Leva, A. (2006). Modelling of thermo-hydraulic power generation processes using Modelica. *Mathematical and Computer Modeling of Dynamical Systems*, *12*, 19–33.

[12] Casella, F., Mathijssen, T., Colonna, P., & van Buijtenen, J. (2013). Dynamic modeling of organic Rankine cycle power systems. *Journal of Engineering for Gas Turbines and Power*, *135*, 042310.

[13] Colonna, P., Casati, E., Trapp, C., Mathijssen, T., Larjola, J., Turunen-Saaresti, T., & Uusitalo, A. (2015). Organic Rankine cycle power systems: From the concept to current technology, applications, and an outlook to the future. *Journal of Engineering for Gas Turbines and Power*, *137*, 1–19.

[14] Douglas-Westwood (2010). *Offshore Wind Asessment For Norway: Final report*. Report The Research Council of Norway.

[15] Grottke, M., Sun, H., Fricks, R. M., & Trivedi, K. S. (2008). Ten fallacies of availability and reliability analysis, . (pp. 187–206).

[16] Haglind, F., & Elmegaard, B. (2009). Methodologies for predicting the part-load performance of aero-derivative gas turbines. *Energy*, *34*, 1484–1492.

[17] Haileselassie, T. M., Molinas, M., Undeland, T. et al. (2008). Multi-terminal VSC-HVDC system for integration of offshore wind farms and green electrification of platforms in the North Sea. In *Proceedings of Nordic Workshop on Power and Industrial Electronics*. Espoo, Finland.

[18] He, W., Jacobsen, G., Anderson, T., Olsen, F., Hanson, T. D., Korpås, M., Toftevaag, T., Eek, J., Uhlen, K., & Johansson, E. (2010). The potential of integrating wind power with offshore oil and gas platforms. *Wind Engineering*, *34*, 125–138.

[19] Hetland, J., Kvamsdal, H. M., Haugen, G., Major, F., Kårstad, V., & Tjellander, G. (2009). Integrating a full carbon capture scheme onto a 450MW$_e$ NGCC electric power generation hub for offshore operations: Presenting the Sevan GTW concept. *Applied Energy*, *86*, 2298–2307.

[20] Incropera, F. P., DeWitt, D. P., Bergman, T. L., & Lavine, A. S. (2007). *Fundamentals of Heat and Mass Transfer*. Jefferson City, United States of America: John Wiley & Sons, Inc. ISBN: 9780470501979.

[21] International Electrotechnical Commission - IEC (2005). *Wind turbines - Part 1: Design requirements*. Technical Report International Electrotechnical Commission.

[22] Jones, P., Stendius, L., & Sweden, A. (2006). The challenges of offshore power system construction. Troll A, electrical power delivered successfully to an oil and gas platform in the North Sea. In *Proceedings of European Wind Energy Conference & Exhibition*. Athens, Greece.

[23] Jonkman, J. M., Butterfield, S., Musial, W., & Scott, G. (2009). *Definition of a 5-MW reference wind turbine for offshore system development*. Technical Report National Renewable Energy Laboratory.

[24] Kloster, P. (1999). Energy optimization on offshore installations with emphasis on offshore combined cycle plants. In *Proceedings of Offshore Europe Conference*. Aberdeen, Great Britain.

[25] Kurzke, J. (2004). *Component map collection 2, Compressor and turbine maps for gas turbine performance computer programs. www.gasturb.de/ [accessed: 19/09/2013]*. Germany.

[26] Kurzke, J. (2005). How to create a performance model of a gas turbine from a limited amount of information. In *Proceedings of ASME Turbo Expo 2005*. Reno-Tahoe, Nevada.

[27] LORC Knowledge (2012). www.lorc.dk/offshore-wind-farms-map/bard-offshore-1, [accessed: 21/10/2015].

[28] M, K., & JK, K. (2012). Offshore wind power basics. *Comprehensive Renewable Energy*, *Volume 2*, 431–468.

[29] Mann, J. (1998). Wind field simulation. *Probabilistic engineering mechanics*, *13*, 269–282.

[30] Martin Wall, S. F., Richard Lee (2006). *Offshore gas turbines (and major driven equipment) integrity and inspection guidance notes*. Technical Report ESR Technology Ltd.

[31] Marvik, J. I., Øyslebø, E. V., & Korpås, M. (2013). Electrification of offshore petroleum installations with offshore wind integration. *Renewable Energy*, *50*, 558–564.

20

[32] Ministry of the Environment (2012). www.regjeringen.no, [accessed: 21/10/2015].

[33] Nguyen, T.-V., Pierobon, L., Elmegaard, B., Haglind, F., Breuhaus, P., & Voldsund, M. (2013). Exergetic assessment of energy systems on North Sea oil and gas platforms. *Energy*, *62*, 23–36.

[34] Norwegian Technology Centre (2007). *Electrical Systems NORSOK STANDARD E-001*. Technical Report Norwegian Technology Centre.

[35] Øye, S. (1996). Flex4 simulation of wind turbine dynamics. In *Proceedings of the 28th IEA Meeting of Experts Concerning State of the Art of Aeroelastic Codes for Wind Turbine Calculations*. Kongens Lyngby, Denmark.

[36] Pierobon, L., & Haglind, F. (2014). Design and optimization of air bottoming cycles for waste heat recovery in off-shore platforms. *Applied Energy*, *118*, 156–165.

[37] Pierobon, L., Iyengar, K., Breuhaus, P., Kandepu, R., Hana, M., & Haglind, F. (2014). Dynamic performance of power generation systems for off-shore oil and gas platforms. In *Proceedings of ASME Turbo Expo 2014*. Düsseldorf, Germany.

[38] Pierobon, L., Kandepu, R., & Haglind, F. (2012). Waste heat recovery for offshore applications. In *Proceedings of ASME 2012 International Mechanical Engineering Congress and Exposition*. Houston, Texas.

[39] Pierobon, L., Nguyen, T.-V., Larsen, U., Haglind, F., & Elmegaard, B. (2013). Multi-objective optimization of organic Rankine cycles for waste heat recovery: Application in an offshore platform. *Energy*, *58*, 538–549.

[40] Prez, J. M. P., Mrquez, F. P. G., Tobias, A., & Papaelias, M. (2013). Wind turbine reliability analysis. *Renewable and Sustainable Energy Reviews*, *23*, 463 – 472.

[41] Romeu, J. L. (). *Understanding series and parallel systems reliability* volume 11.

[42] Schobeiri, M. (2005). *Turbomachinery flow physics and dynamic performance*. Berlin, Germany: Springer Berlin. ISBN: 9783540223689.

[43] Statoil (2009). www.statoil.com, [accessed: 21/10/2015].

[44] Stodola, A. (1922). *Dampf- und Gasturbinen: Mit einem Anhang über die Aussichten der Wärmekraftmaschinen*. Berlin, Germany: Springer Berlin. ISBN: 7352997563.

[45] Undrum, H., Bolland, O., & Aarebrot, E. (2000). Economical assessment of natural gas fired combined cycle power plant with CO_2 capture and sequestration. In *Proceedings of the 5th International Conference on Greenhouse Gas Control Technologies*. Cairns, Australia.

[46] Veres, J. P. (1994). *Centrifugal and Axial Pump Design and Off-Design Performance Prediction*. Technical Report NASA Sunnyvale, United States of America. Technical Memorandum 106745.
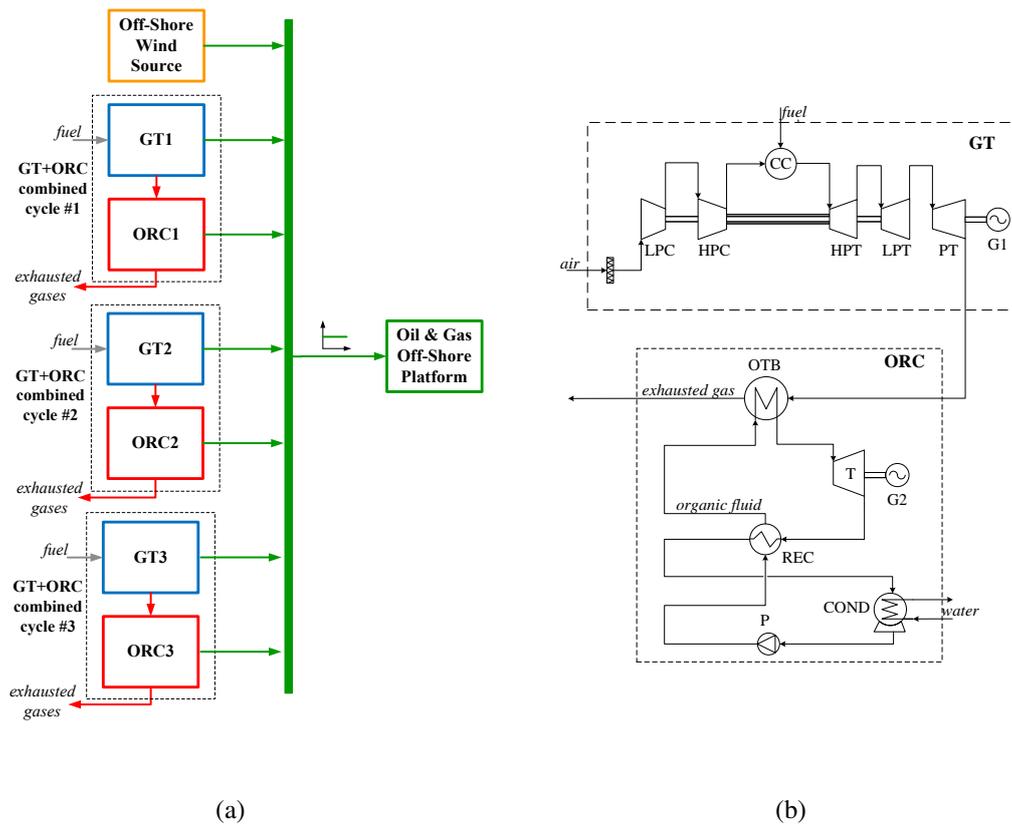
Figures

21

Figure 1: Layout of the power system considered as case study. Figure 1(a) Integration of gas turbines, organic Rankine cycle units and wind farm with the electric grid. 1(b) Combined cycle unit configuration.
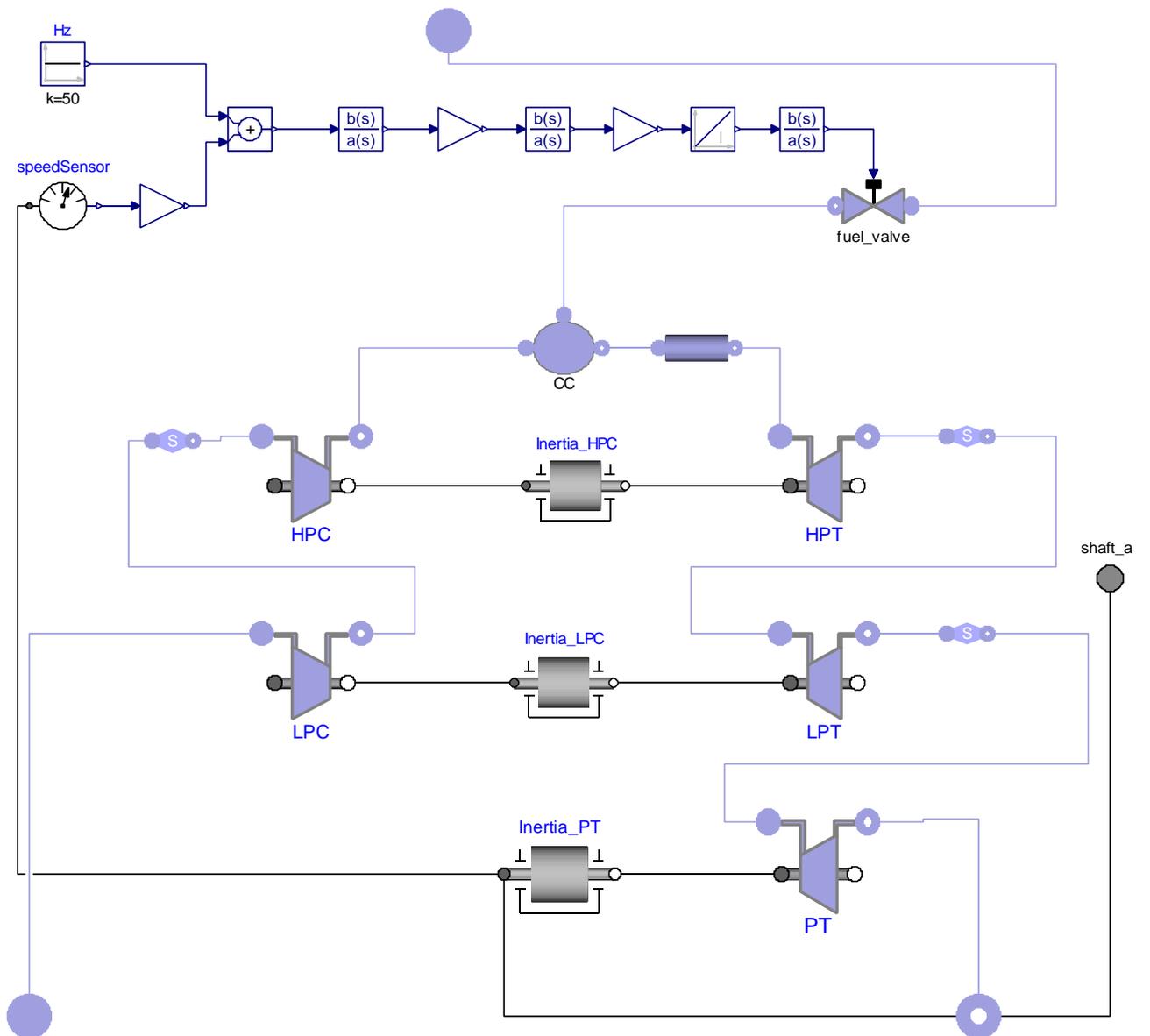
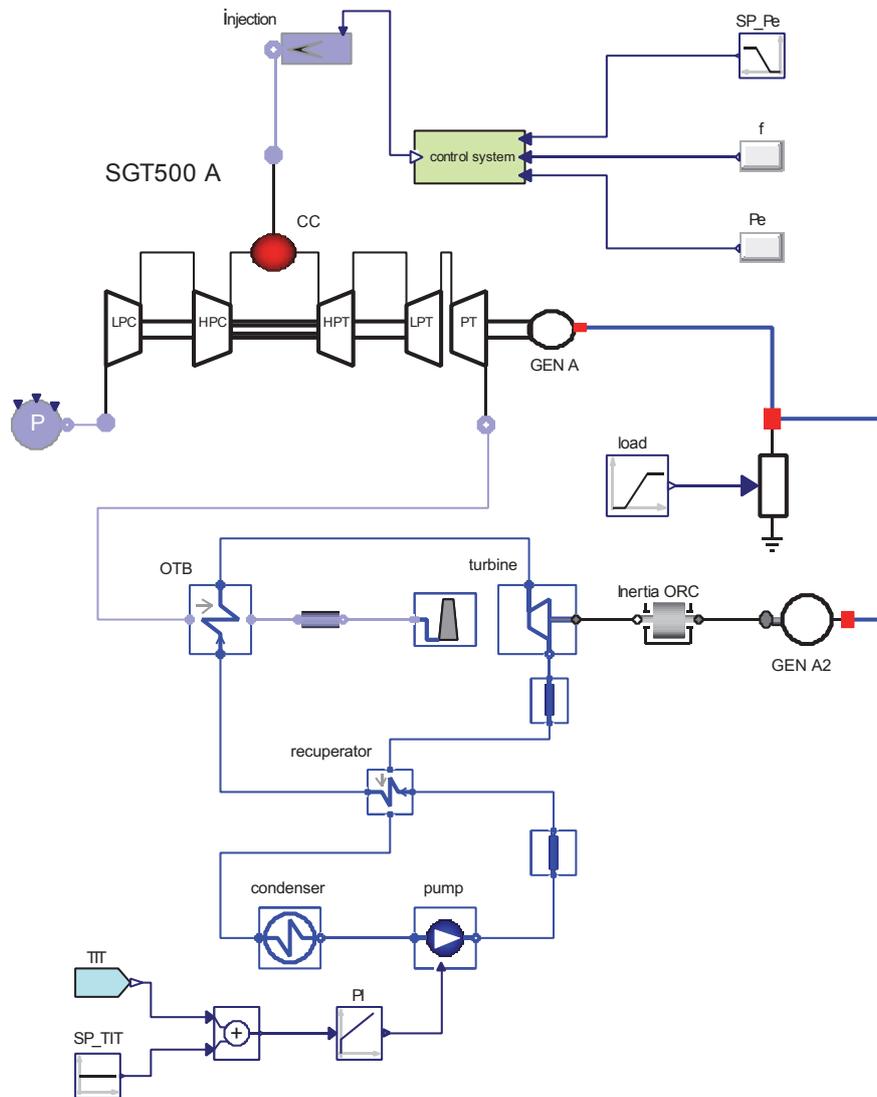Figure 2: Object diagram of the gas turbine sub-system model.

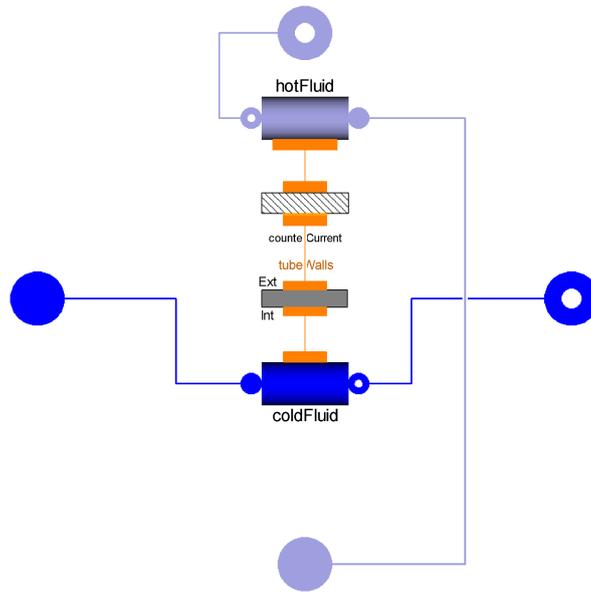Figure 3: Object diagram of the combined cycle unit.

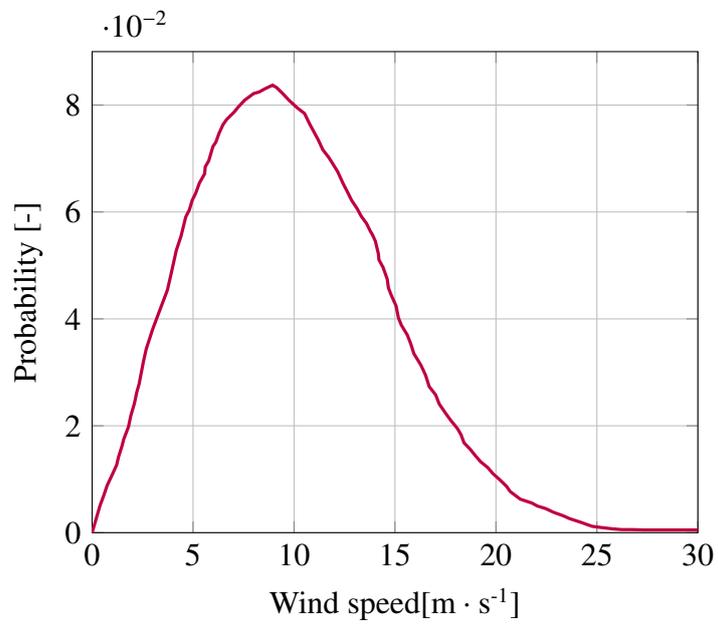Figure 4: Modelica object diagram of the once-through heat exchanger model.
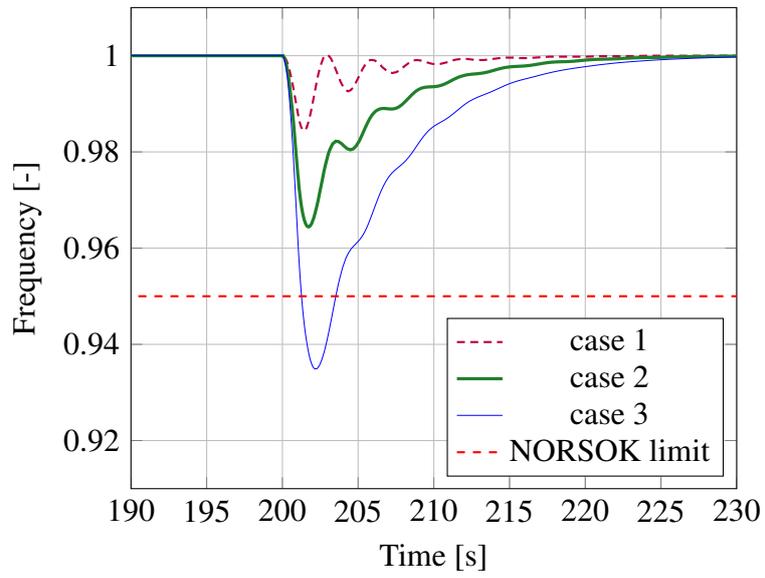

Figure 5: Probability distribution of wind speed.

Figure 6: Frequency in per unit as a function of time for the analyzed cases.
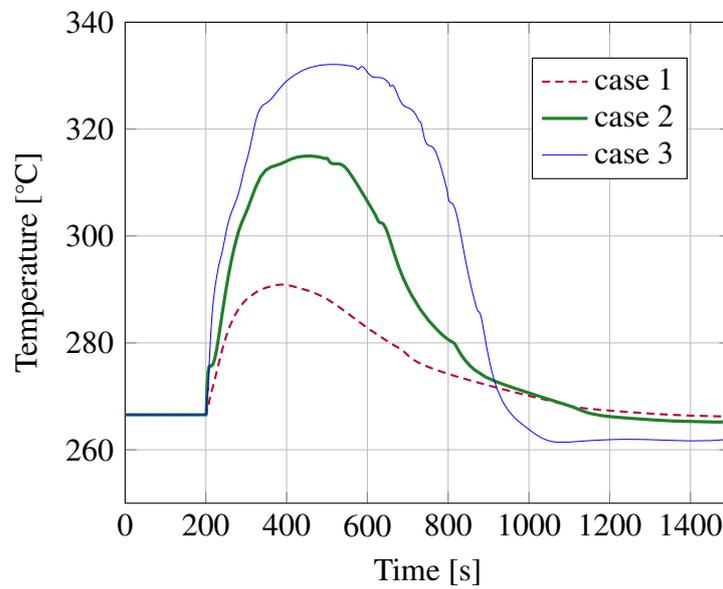
Figure 7: Maximum temperature of the organic fluid in the thermodynamic cycle as a function of time for the analyzed cases.
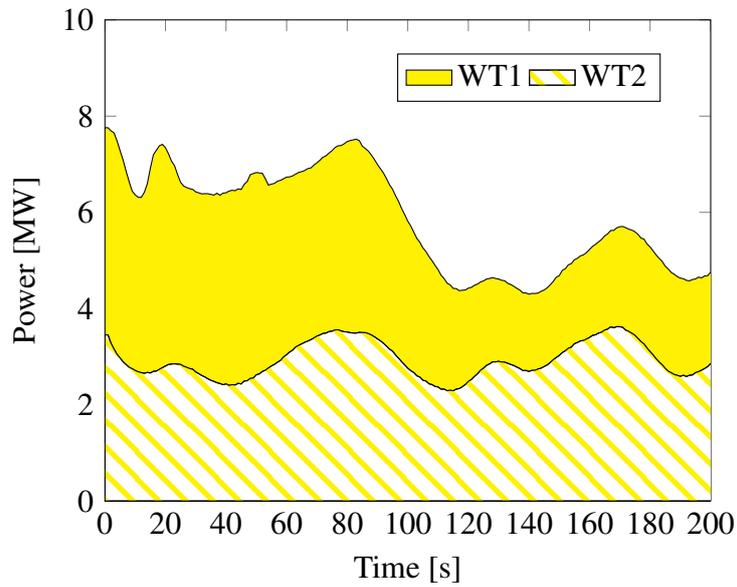
Figure 8: Electric power of the two wind turbines as a function of time.

(a)

(b)
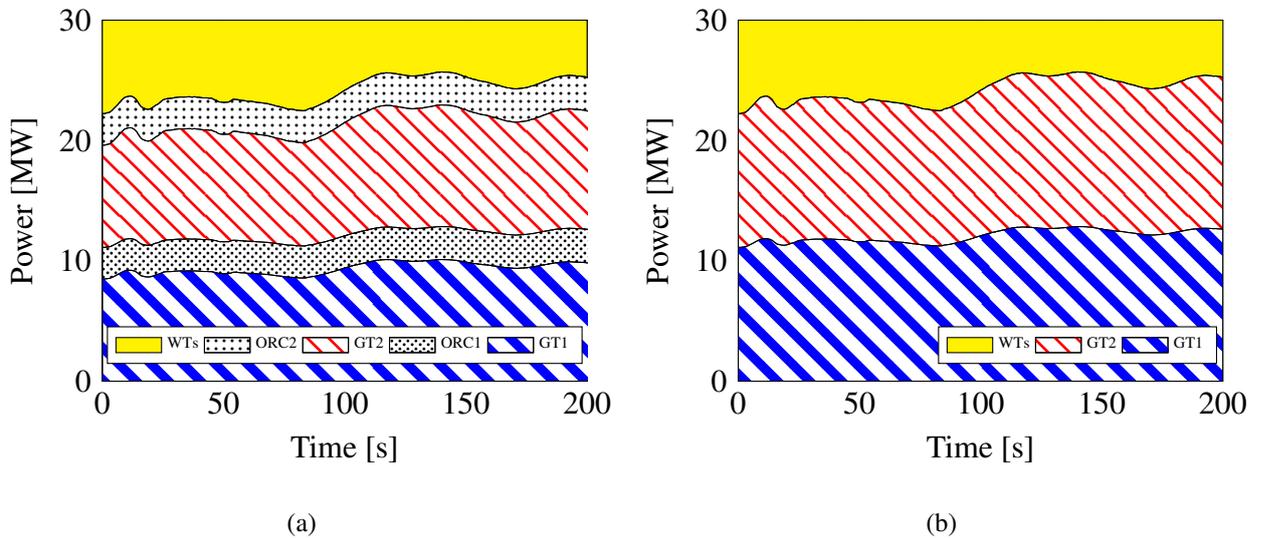
Figure 9: Power of the electric generators connected to the grid as a function of time. 9(a): Two gas turbines, two organic Rankine cycle units and the wind mill. 9(b): Two gas turbines and the wind mill.
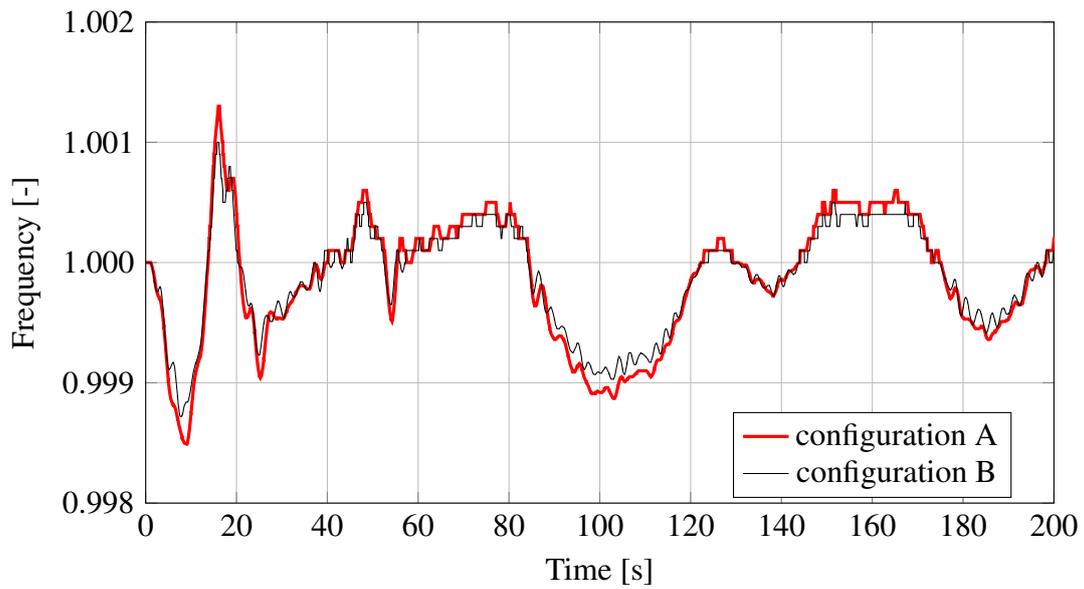
Figure 10: Frequency in per unit as a function of time. In configuration A, the gas turbines, the organic Rankine cycle units and the wind mill supply the electric grid. Conversely, configuration B entails the use of the gas turbines and the wind mill.
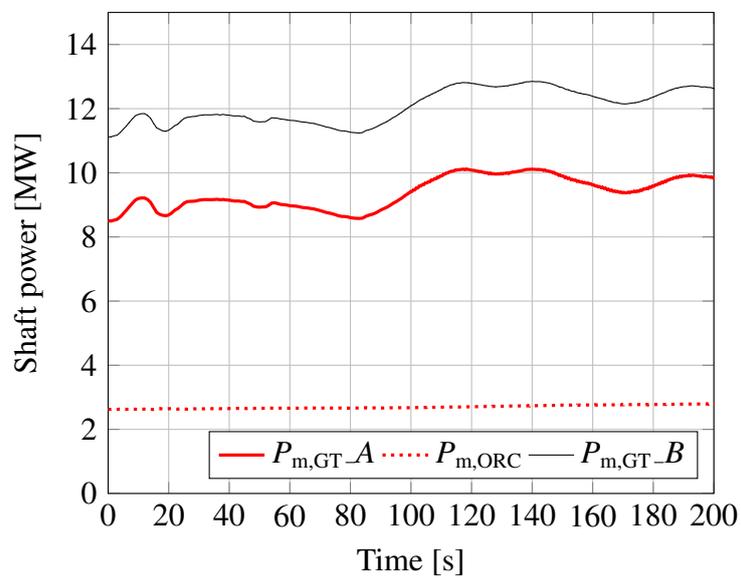

Figure 11: Gas turbine and organic Rankine cycle mechanical power in configuration A and gas turbine mechanical power in configuration B as a function of time.
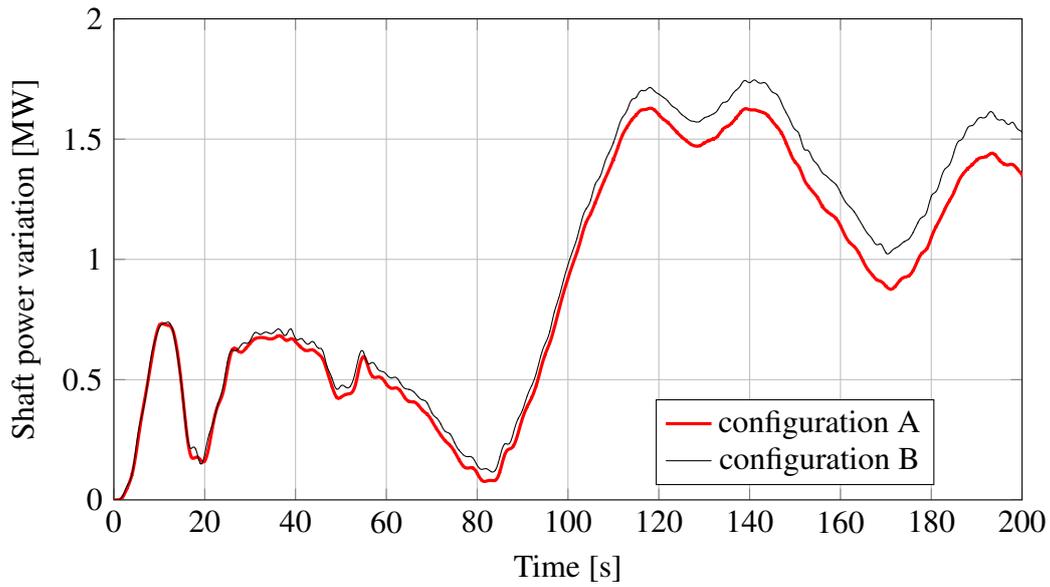
.

28

Figure 12: Variation of the mechanical power supplied by one gas turbine with respect to the steady-state value for configuration A and B.
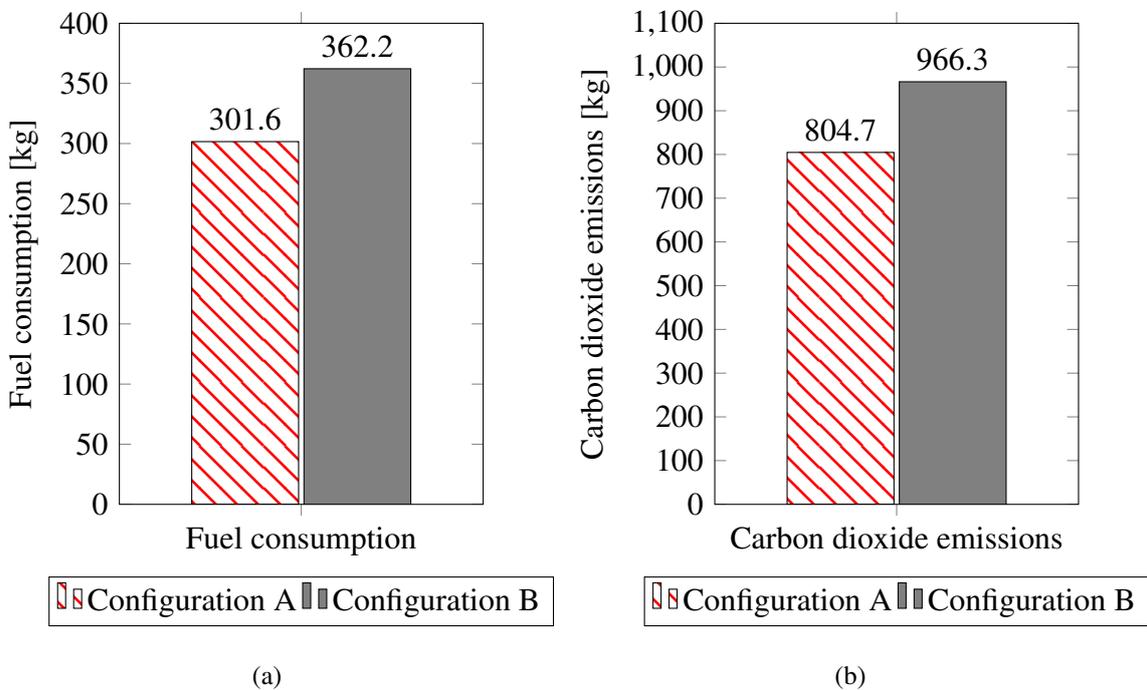

(a)

(b)

Figure 13: Fuel savings (13(a)) and carbon dioxide emissions (13(b)) of the gas turbines, the organic Rankine cycle units and the wind mill (configuration A) and for the gas turbines and the wind mill (configuration B).
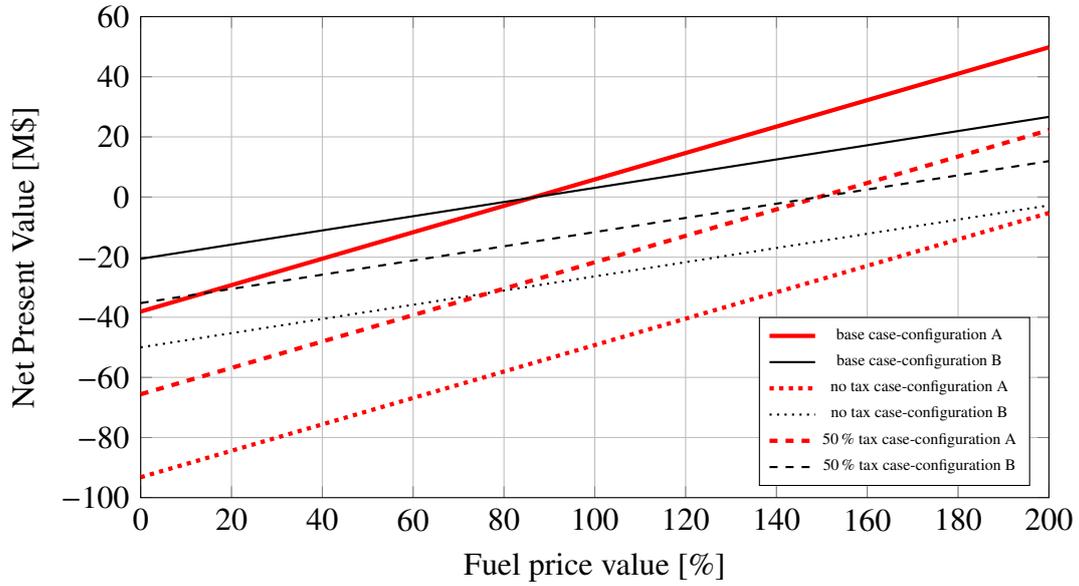
Figure 14: Net present value for configuration A and B as a function of the fuel price variation respect the base case (in percentage): effects of the CO_2 tax value decreasing.
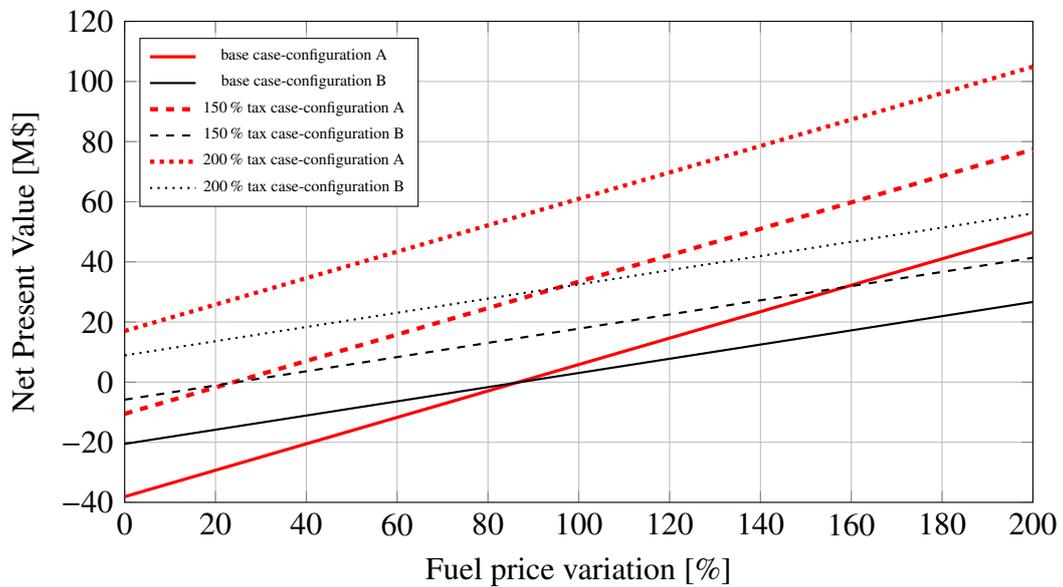

Figure 15: Net present value for configuration A and B as a function of the fuel price variation respect the base case (in percentage): effects of the CO_2 tax value increasing.

Tables

Table 1: Design specificationsprovided by the manufacturer for the twin-spool gas turbine considered as topping unit.

Model	Siemens SGT-500
Turbine inlet temperature	850 °C
Exhaust gas temperature	379.2 °C
Exhaust gas mass flow	91.5 kg · s^{-1}
Electric power output	16.5 MW
Thermal efficiency	31.3 %

Table 2: Design variables used to parametrize the dynamic model of the organic Rankine cycle system, obtained as described in [39].

Component	Parameters
ORC thermal efficiency	21.8 %
ORC power output	4.8 MW
Once-through boiler	
Volume (cold side)	10.3 m^{-3}
Volume (hot side)	51.5 m^{-3}
Weight (metal walls)	45.4 t
UA-value	420.7 kW $\cdot$ K^{-1}
Recuperator	
Volume (cold side)	1.18 m^{-3}
Volume (hot side)	13.24 m^{-3}
Weight (metal walls)	10.23 t
UA-value	390 kW $\cdot$ K^{-1}
Turbine	
Throat flow passage area	0.040 m^{-2}
Isentropic efficiency	81.6 %
Electric generator efficiency	98 %
Pump	
Delivery pressure	2928 kPa
Inlet pressure	36 kPa
Isentropic efficiency	72 %